

# Analysis of selective vaporization behavior in laser melting of magnesium alloy by plume deposition

GUAN YINGCHUN,<sup>1,2</sup> ZHOU WEI,<sup>1,2</sup> ZHENG HONGYU,<sup>2</sup> LI ZHONGLI,<sup>2</sup> SENG HWEE LENG,<sup>3</sup> AND HONG MINGHUI<sup>4</sup>

<sup>1</sup>Nanyang Technological University, Singapore

<sup>2</sup>Singapore Institute of Manufacturing Technology, Singapore

<sup>3</sup>Institute of Materials Research & Engineering, Singapore

<sup>4</sup>National University of Singapore, Singapore

(RECEIVED 11 April 2013; ACCEPTED 18 June 2013)

## Abstract

Laser surface melting is one of the most important processes in laser material processing. Selective vaporization of alloying elements in laser melting offers fundamental understanding of laser processing on metallic alloys. This work provides linkage between laser melting and material properties using secondary ion mass spectrometry (SIMS) for tiny vaporized species in laser-generated plume and energy dispersive spectroscopy (EDS) for solid solution range in molten pool, both qualitatively and quantitatively (up to hundreds of micron). Silicon wafer was used to collect the generated plume. Chemical analysis was carried out on top surface and sub-surface of the deposited plume. Transport behavior as well as distribution of the vaporized species inside the plume was further proposed.

**Keywords:** laser processing; selective vaporization; secondary ion mass spectrometry; magnesium alloy; surface modification

## 1. INTRODUCTION

Selective vaporization is common but complex phenomenon during laser-material interaction due to physical and chemical processes that occur between incident laser light and irradiated surface within a very short time period (David & Debroy, 1992; Steen, 2003). Previous work has been focused on analytical study of ablated particles (Zhao & Debroy, 2001; Matsuta *et al.*, 2004), laser induced plasma emission spectrometry or laser induced breakdown spectroscopy (Mochizuki *et al.*, 1991; Jandaghi *et al.*, 2009; Goodall *et al.*, 1995), and theoretical calculation of laser-generated plume, to investigate mechanism of selective vaporization and its effect on materials properties (Zhao & Debroy, 2001; He *et al.*, 2004). In laser processing of metallic alloys, it is known that selective vaporization occurs due to different vaporization rates of alloying elements at high temperature and excess pressure, and it determines surface chemistry of laser-treated layer (Steen, 2003; He *et al.*, 2004; Moon & Metzbower, 1983; Cieslak & Fuerschbach, 1988; Willmott & Huber, 2000; Cao *et al.*, 2003; Stasic *et al.*, 2009). Selective

vaporization in laser welding has been shown to affect mechanical properties, corrosion resistance, and hot crack susceptibility of the weldment significantly (David & Debroy, 1992; Steen, 2003; He *et al.*, 2004; Moon & Metzbower, 1983; Cieslak & Fuerschbach, 1988; Willmott & Huber, 2000; Cao *et al.*, 2003).

As one of the most important techniques involved in laser processing, laser surface melting on metallic materials offers fundamental way to understand different laser methods on metallic alloys for various purposes, such as welding and joining, cutting and drilling, cladding and alloying, etc. In recent years, driven by unique advantages as structure materials in industries and as implant materials in bio-medical area, laser processing on Mg alloys has attracted increasing attention to improve their surface performance (Kutz, 2002; Witte, 2010; Song, 2010; Zhang *et al.*, 2011; Guan *et al.*, 2009a; 2009b; 2009c; Ignat *et al.*, 2004). Our previous work indicates that enhanced Al concentration in the molten pool caused by laser surface melting plays an important role in determining the improved bio-corrosion resistance and surface wettability of laser melt Mg alloy (Zhang *et al.*, 2011; Guan *et al.*, 2009a; 2009b; 2009c). However, the linkage between selective vaporization in laser melting and extended solid solution range in molten pool is still missing.

Address correspondence and reprint requests to: Y.C. Guan, Nanyang Technological University, 50 Nanyang Avenue, Singapore 639798.  
E-mail: [guan0013@e.ntu.edu.sg](mailto:guan0013@e.ntu.edu.sg)

This work aims to study selective vaporization of alloying elements induced by millisecond pulse Nd:YAG laser surface melting on AZ91D Mg alloy. Si wafer is used to collect laser-generated plume, and chemical investigation using SIMS is performed by analyzing tiny vaporized species at top-surface and sub-surface of the deposited plume. Enrichment of alloying element in the molten pool is studied by EDS. By characterizing surface morphology and chemical composition of the deposited plume and molten pool, mechanism of selective vaporization is further discussed.

## 2. EXPERIMENTAL PROCEDURES

The material studied was an as-cast AZ91D Mg alloy with the following chemical composition (wt. %): Al 8.97, Zn 0.78, Mn 0.31, Si 0.023, Cu 0.002, Ni 0.0005, and Mg balance. Millisecond pulse Nd:YAG laser (with wavelength of 1064 nm) was used under the following parameters at atmospheric pressure and room temperature in air: power density  $3.82 \times 10^4 \text{ W/cm}^2$ , frequency 100 Hz, pulse duration 1.0 ms, and single firing pulse. Microstructural features of the molten pool were studied using JEOL 5600 LV SEM equipped with EDS. The EDS measurements provided information on the chemical composition.

A novel aspect of the experiment was to make use of Si substrate to collect the plume generated during laser irradiation, as shown in Figure 1. The distance between the Si substrate and the laser firing point on Mg sample was 3 mm. The Si substrate was H-terminated by cleaning in organic solvents and subsequent immersion in HF aqueous solution (Li *et al.*, 2004). The plume deposited on the Si substrate was studied using SEM and further analyzed using time-of-flight secondary ion mass spectrometry (TOF-

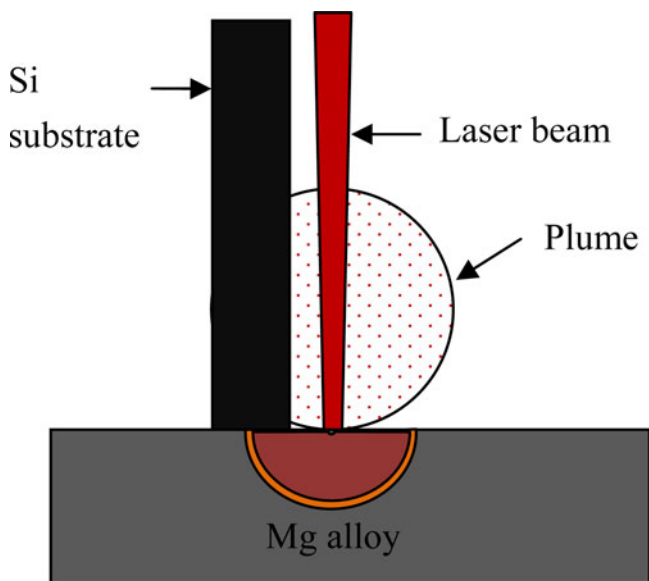


Fig. 1. (Color online) Diagram showing experimental set-up for collecting plume generated by laser firing.

SIMS). Scan area of spectrometry on Si was nearly  $200 \mu\text{m} \times 200 \mu\text{m}$ . Mass-resolved images (MRIs) for chemical mapping of vaporized elements were reconstructed from  $500 \mu\text{m} \times 500 \mu\text{m}$  in the deposited plume, and depth profile was performed within the MRIs area as  $150 \mu\text{m} \times 150 \mu\text{m}$ . Chemical content of elements was calculated by normalizing ion intensity to sum of major elements in the substrate.

## 3. RESULTS AND DISCUSSIONS

Figure 2a shows typical microstructure and chemical distribution in AZ91D Mg alloy before and after laser surface melting. Bulk and lamellar  $\beta\text{-Mg}_{17}\text{Al}_{12}$  phase distributed non-homogeneously in  $\alpha\text{-Mg}$  matrix is indicated in the as-received microstructure of substrate. In the molten pool, solidification microstructure consisted of cellular/dendrite structure, which was derived from refined  $\alpha\text{-Mg}$  and  $\beta\text{-Mg}_{17}\text{Al}_{12}$  phases, are observed (Guan *et al.*, 2009a; 2009b; 2009c). The distribution of main elementary compositions Mg and Al based on EDS analysis revealed that average Al content increased in the molten pool. Quantitative analyses of the micrographs confirmed that Al content was in the range of 10.7–12.1 wt. % and was enriched at the dendrite/cellular boundaries in the range of 30.8–33.3 wt. %, which were higher than 9.0 wt. % in the untreated substrate. The enrichment of Al in the molten pool has been validated to be a key factor responsible for improved bio-corrosion resistance and surface wettability of laser-melt AZ91D Mg alloy, and the detailed information is not repeated here (Song, 2010; Guan *et al.*, 2009b; 2009c).

Figure 2b shows surface morphology of the plume deposited on Si substrate after laser firing. The deposited plume revealed an ellipse shape with dimension around  $500 \mu\text{m} \times 1500 \mu\text{m}$ , and the average thickness was measured as 322 nm in 15 different points of the plume. Location of MRIs and depth profile analysis are also illustrated in Figure 2b. A few liquid ejected droplets of molten material was observed, indicating phase explosion phenomenon with a mixture of liquid and vapor during laser processing (Steen, 2003; Goodall *et al.*, 1995).

The MRIs results are shown in Figure 2c. According to color contrast of Si, boundary between the deposited plume, and the Si substrate was indicated as a white line. According to color contrast of Si, boundary between the deposited plume and the Si substrate was indicated as a white line since chemical images were generated by collecting mass spectrum at every pixel during TOF-SIMS measurement. It is further noted that concentration of Mg species is much higher than that of Al and Zn inside the plume. Moreover, distribution of Mg species is found to be uniform in the whole area, while distribution of Al species increases with the distance starting from the boundary. Zn species are very few in the deposited plume. The signal of Mg, Al, and Zn species below the boundary line was due to edge effect during deposition process.

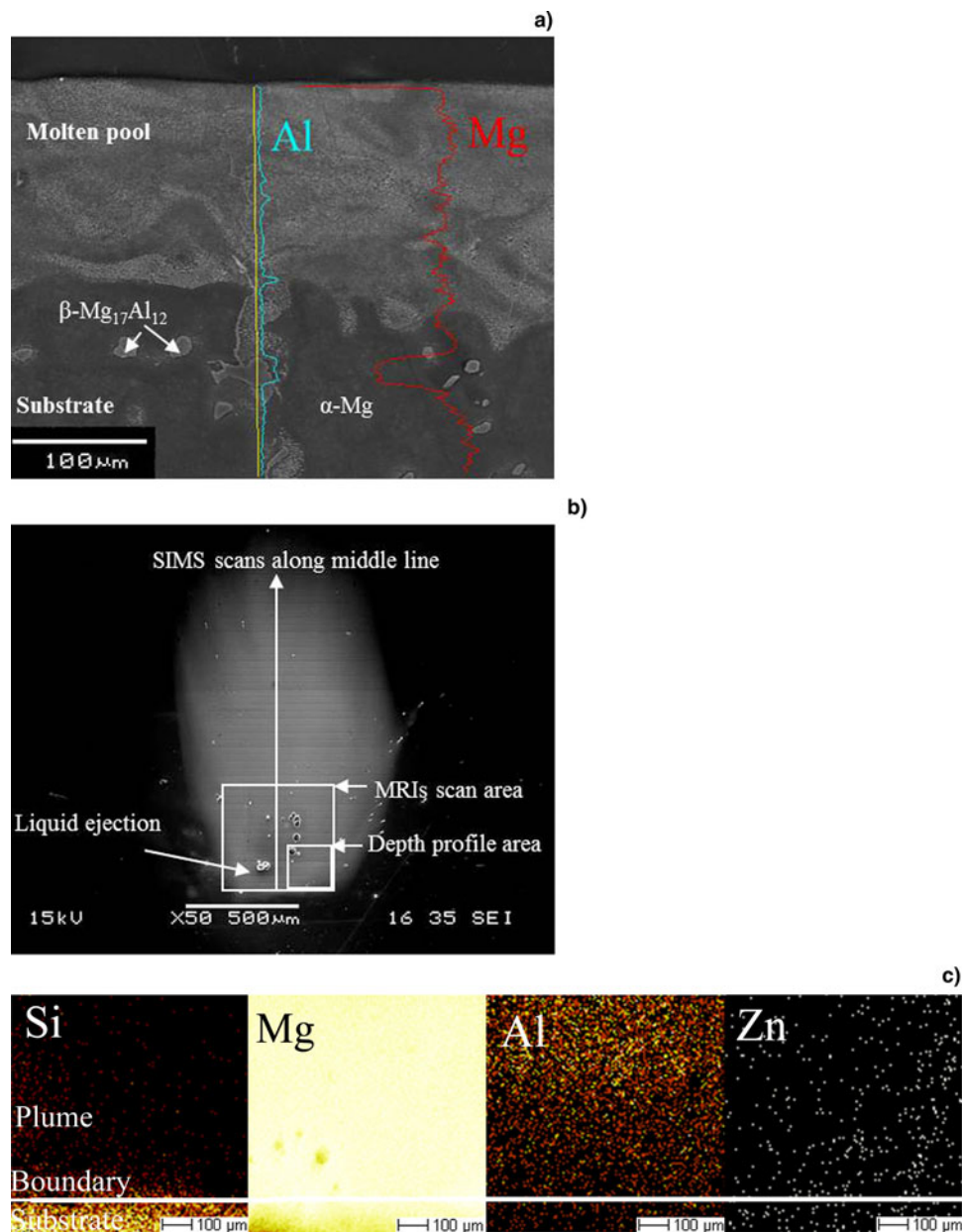


**Fig. 2.** (Color online) (a) EDS line scan indicating distribution of main elements Al and Mg in the molten pool of AZ91D Mg alloy induced by laser surface melting. (b) SEM image indicating morphology of deposited plume on Si wafer and locations of SIMS analysis. (c) MRIs showing chemical mapping of main elements in (b).

The normalized Mg and Al contents in the depth profile area are shown in Figure 3. Figure 3a provides schematic diagram of cross section view for depth profile measurement on different positions of the deposited plume. Figure 3b shows the ratio of Mg:Al contents along the plume thickness through depth profile measurements. At the surface, the ratio was calculated as 61.3:1, which was much higher than base metal composition as 10:1. With the increasing sputtering time, Mg concentration decreased rapidly, while Al concentration increased. When it reached to the sub-surface indicated as position b, Al was enriched and the ratio of Mg:Al reduced to 9.66:1. When further increased to position

c, the ratio of Mg:Al reduced to 1.21:1, and the final ratio of Mg:Al was 3:1 at position d due to very low Mg and Al contents. The corresponding sub-surface locations of b, c, and d were estimated to be 181 nm, 265 nm, 1228 nm. In other words, Mg dropped rapidly from the surface (position a) to the sub-surface (position b to position d), while Al increased first and then decreased. Al content was higher than that of Mg in the deep sub-surface, as indicated from position c to position d. Therefore, at the initial stage of vaporization and deposition process, the number of Mg species deposited on Si sheet was less than that of Al. With the increasing time, Mg species increased rapidly compared to that of Al. At the

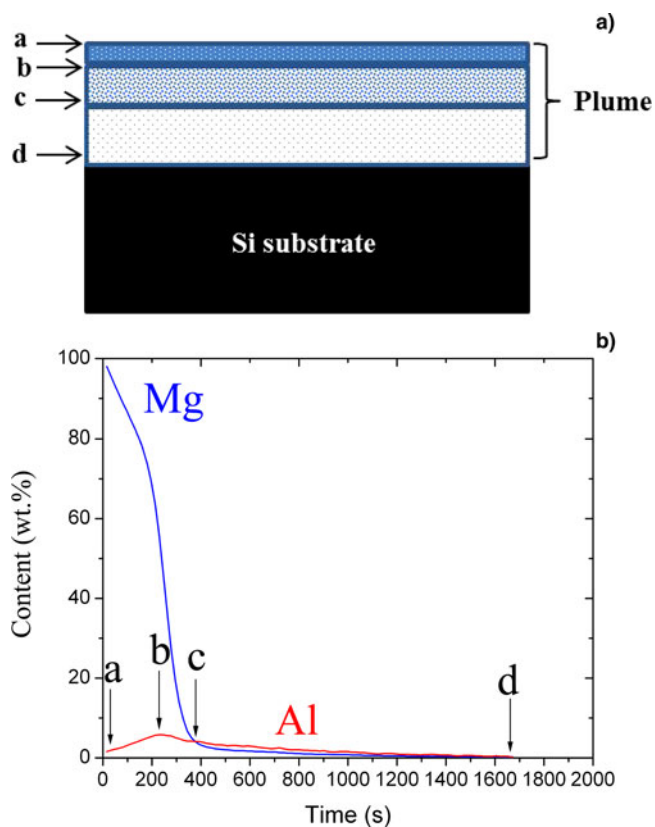


**Fig. 3.** (Color online) (a) Schematic diagram of cross section view for TOF-SIMS depth profile measurement on the deposited plume above Si substrate, while a, b, c and d showing different positions from top surface towards sub-surface of the deposited plume; (b) Chemical content distribution of vaporized Mg and Al species at bottom of deposited plume with sputtering time using TOF-SIMS depth profile. It shows that Mg:Al ratio is very low at initial deposition of laser-generated plume on Si substrate (d), and it changes rapidly with the process due to high concentration of Mg compared to Al (c to a).

final stage, Mg species remained increasing, while Al species dropped to nearly zero.

The chemical content distribution of vaporized Mg and Al species on the surface of whole plume in Figure 2b were further calculated, and listed in Table 1. Total length of the plume was measured as 1500  $\mu\text{m}$  as shown in Figure 2b, and it was divided into three categories according to the rapid change of Mg distribution: (1) 500  $\mu\text{m}$  and below,

**Table 1.** Chemical content distribution of vaporized Mg and Al species on whole surface of the deposited plume using TOF-SIMS scanning

Distance ( $\mu\text{m}$ )	Mg content (wt. %)	Al content (wt. %)	Mg/Al
200	96.6	1.5	64.9
500	93.8	1.8	51.9
800	76.3	3.3	23.0
1100	5.2	0.5	10.3
1400	0.3	0.3	0.9

(2) 500–800  $\mu\text{m}$ , and (3) 800  $\mu\text{m}$  and above. In bottom plume I from 200  $\mu\text{m}$  to 500  $\mu\text{m}$ , Mg did not decrease too much, and the average ratio of Mg:Al was more than 50:1. This is in agreement with the results in Figures 2b and 3b, and it indicates that the vaporization of Mg is far exceeded than that of Al. In middle plume I from 500  $\mu\text{m}$  to 800  $\mu\text{m}$ , Al concentration increased from 1.8 wt. % to 3.3 wt. % while Mg concentration started to drop, which indicates that Al “flies” further compared that of Mg (similar to MRIs in Fig. 2c). In top plume 2 from 800  $\mu\text{m}$  to 1400  $\mu\text{m}$ , both Mg and Al dropped significantly rapidly, from 76.3 wt. % to 0.3 wt. % and from 3.3 wt. % to 0.3 wt. %, respectively. In addition, the ratio of Mg:Al decreased significantly from 23.0:1 to 0.9:1. It should be noted that Al distribution in deposited plume has similar trend for both depth profile and top surface measurement, which increased first and then dropped. The reason for such phenomenon will be explained in the following.

The ratio of Mg:Al was 10:1 in the base composition of AZ91D Mg alloy, and vaporization rate of Mg was calculated as almost two orders of magnitude greater than that of Al according to Zhao and Debroy (2001) and He *et al.* (2004). Therefore, the combined effect of different vaporization rate and original chemical composition resulted in the great ratio of Mg:Al in the deposited plume, as shown in Figure 3 and Table 1.

Distribution of vaporized Mg and Al species in the plume is further explained in Figure 4. At the bottom of plume, which was indicated as near-field region, density of vaporized species was very high and local vapor pressure exceeded ambient pressure when the plume generated from molten

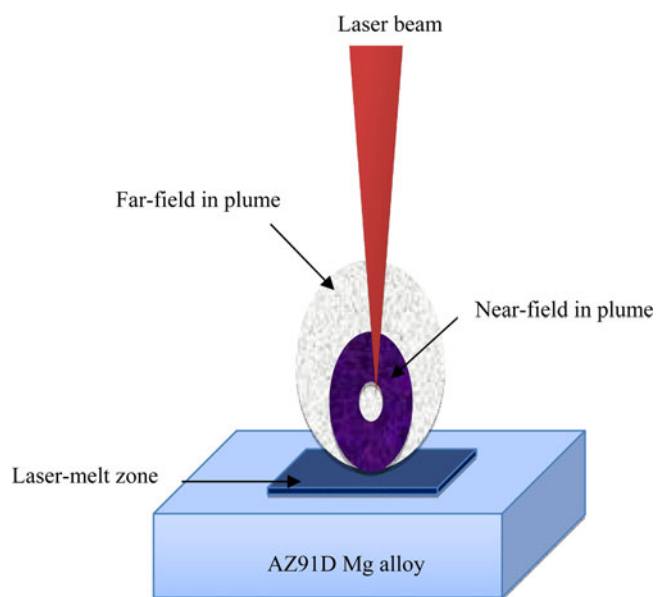


**Fig. 4.** (Color online) Schematic showing near-field region and far-field region in the plume generated from molten pool surface during laser irradiation. Dark spots inside the plume indicates high diffusivity of Al vapors compared to the remaining Mg vapors. Liquid droplets of molten materials are not presented.

pool surface (Steen, 2003; Yoo *et al.*, 2000). According to Table 1, height of the near-field region was estimated as 800  $\mu\text{m}$ . When the plume expanded into surrounding environment, vapor pressure decreased significantly. Simultaneously, pressure difference between the core region and the atmosphere would lead to a far-field region at the top of the plume (Cieslak & Fuerschbach, 1988; Yoo *et al.*, 2000). Correspondingly, the density of vaporized species decreased rapidly in such far-field region, and this was shown as low contents of Mg and Al from 1100  $\mu\text{m}$  to 1400  $\mu\text{m}$  in Table 1. Such conclusion is in strong agreement with the findings of Li (2004), who has observed three different regions of deposited plume in polyimide film and polycarbonate substrates. Our result also supports Debroy's calculation in terms of experimental evidence aspect that vaporization is concentrated in a small active region where local vapor pressure exceeds ambient pressure under laser beam (Zhao & Debroy, 2001; He *et al.*, 2004).

The discrepancy distribution of Mg and Al both at the top surface and in the sub-surface of the deposited plume was proposed to transport rate of vaporized species from the molten pool surface to the plume. The transport rate of vaporized alloying elements is reported to be depended on nature of boundary layer and diffusivities of vaporized species (Willmott & Huber, 2000; Collur *et al.*, 1987) Based on Chapman-Enskog theory (Collur *et al.*, 1987), the diffusivities of Mg and Al vapors in Ar gas at various temperatures are calculated, and the diffusivity of Al is nearly two to three times than that of Mg at high temperature range from 2500 K to 3500 K. In the near-field region, high diffusivity of Al results in its vaporized species "fly" far than that of Mg in both bottom and middle of plume due to high temperature. In the far-field region, however, Al concentration decreases correspondingly when temperature drops significantly, as shown in Figures 2c, 3, and Table 1. Therefore, we suggest that the reason for Al distribution in the deposited plume was caused by higher transport rate of vaporized Al species during vaporization and deposition process, especially in the near-field region of plume.

#### 4. CONCLUSIONS

Investigating chemical distribution of vaporized alloying elements in the laser-generated plume is useful for mechanism analysis of selective vaporization during laser processing. TOF-SIMS analysis was employed to examine a deposited laser-generated plume on Si substrate after laser surface melting on AZ91D Mg alloy. At the initial deposition of the plume on Si substrate, ratio of Mg: Al was measured nearly as 3:1. When it reached to near-field region of the plume, the ratio increases rapidly to more than 50:1. Meanwhile, Al concentration increased largely and the species "fled" far away than that of Mg. As the plume further expanded to far-field region, the ratio of Mg: Al as well as Mg and Al concentration decreased gradually in the deposited plume. It is proposed that selective vaporization of Mg

and Al alloying elements results in high ratio of Mg:Al and high concentration of vaporized Mg species in the laser-generated plume, and transport rate of vaporized Al species is higher than that of Mg due to high diffusivity at high temperature in the near-field region. Results indicate the use of TOF-SIMS technique for top surface and sub-surface analysis of the deposited plume on Si substrate as an additional route for exploring selective vaporization behavior of alloying elements and offering fundamental understanding during laser processing on metallic alloys.

#### ACKNOWLEDGEMENTS

Support by Nanyang Technological University, Ph.D. scholarship and Singapore Institute of Manufacturing Technology, A\*STAR (Agency for Science, Technology and Research, Singapore), Collaborative Research Project U09-M-006SU is gratefully acknowledged.

#### REFERENCES

- CAO, X., WALLACE, W., POON, C. & IMMARIGEON, J.P. (2003). Research and progress in laser welding of wrought aluminum alloys. *Mater. Manuf. Process* **18**, 1–22.
- CIESLAK, M.J. & FUERSCHBACH, P.W. (1988). On the weldability, composition, and hardness of pulsed and continuous Nd:YAG laser welds in aluminum-alloys 6061, 5456, and 5086. *Metall. Trans.* **19B**, 319–329.
- COLLUR, M.M., PAUL, A. & DEBROY, T. (1987). Mechanism of Alloying Element Vaporization During Laser Welding. *Metall. Trans.* **18B**, 733–740.
- DAVID, S.A. & DEBROY, T. (1992). Current issues and problems in welding science. *Sci.* **257**, 497–502.
- GOODALL, P., JOHNSON, S.G. & WOOD, E. (1995). Laser ablation inductively coupled plasma atomic emission spectrometry of a uranium-zirconium alloy: Ablation properties and analytical behavior. *Spectro Acta Part B* **50**, 1823–1835.
- GUAN, Y.C., ZHOU, W. & ZHENG, H.Y. (2009b). Effect of laser surface melting on corrosion behaviour of AZ91D in simulated-modified body fluid. *J. Appl. Electrochem.* **39**, 1457–1464.
- GUAN, Y.C., ZHOU, W. & ZHENG, H.Y. (2009c). Effect of Nd:YAG laser melting on surface energy of AZ91D Mg alloy. *Surf. Rev. Lett.* **16**, 801–806.
- GUAN, Y.C., ZHOU, W., LI, Z.L. & ZHENG, H.Y. (2009a). Study on the solidification microstructure in AZ91D Mg alloy after laser surface melting. *Appl. Surf. Sci.* **255**, 8235–8238.
- HE, X., DEBROY, T. & FUERSCHBACH, P.W. (2004). Composition change of stainless steel during microjoining with short laser pulse. *J. Appl. Phys.* **96**, 4547–4555.
- IGNAT, S., SALLAMAND, P., GREVEY, D. & LAMBERTIN, M. (2004). WE43 and ZE41 Magnesium alloys Characterisation for Laser Applications. *Appl. Surf. Sci.* **225**, 124–134.
- JANDAGHI, M., PARVIN, P., TORKAMANY, M.J. & SABBAGHZADEH, J. (2009). Alloying element losses in pulsed Nd:YAG laser welding of Stainless Steel-316. *J. Phys. D: Appl. Phys.* **42**, 205301.
- KUTZ, M. (2002). *Handbook of Materials Selection*. New York: John Wiley & Sons.

- LI, Z.L., YOW, S.Z., LUI, L., YAKOVLEV, N.L., SUN, Y., SWENSON, E.J. & MORAN, P.M. (2004). SIMS study of plumes generated from laser ablation of polymers. *Appl. Phys. A* **78**, 611–616.
- MATSUTA, H., NAEEM, T.M. & WAGATSUMA, K. (2004). Effect of laser wavelength on the selective vaporization of Cu-Zn alloy in laser ablation at low pressure. *ISIJ International*. **44**, 220–222.
- MOCHIZUKI, T., SAKASHITA, A., TSUJI, T., IWATA, H., ISHIBASHI, Y. & GUNJI, N. (1991). Flow injection technique for determination of thallium, lead and bismuth in nickel-base alloys by inductively coupled plasma mass spectrometry. *Anal. Sci.* **7**, 479–481.
- MOON, D.W. & METZBOWER, E.A. (1983). Laser-beam welding of aluminum alloy-5456. *Welding J.* **62**, S53–S58.
- SONG, G.L. (2010). *Corrosion Behavior of Mg Alloys and Protection Techniques*. Cambridge: CRC Press.
- STASIC, J., GAKOVIC, B., KRMPOT, A., PAVLOVIC, V., TRTICA, M. & JELENKOVIC, B. (2009). Nickel-based super-alloy Inconel 600 morphological modifications by high repetition rate femtosecond Ti:sapphire laser. *Laser Part. Beams* **27**, 699–707.
- STEEN, W.M. (2003). *Laser Material Processing*. London: Springer, London.
- WILLMOTT, P.R. & HUBER, J.R. (2000). Pulsed laser vaporization and deposition. *Rev. Mod. Phys.* **72**, 315–328.
- WITTE, F. (2010). The history of biodegradable magnesium implants: A review. *Acta Biomater.* **6**, 1680–1692.
- YOO, J.H., JEONG, S.H., GREIF, R. & RUSSO, R.E. (2000). Explosive change in crater properties during high power nanosecond laser ablation of silicon. *J. Appl. Phys.* **88**, 1638–1649.
- ZHANG, L.C., KLEMM, D., ECKERT, J., HAOD, Y.L. & SERCOMBEA, T.B. (2011). Manufacture by selective laser melting and mechanical behavior of a biomedical Ti-24Nb-4Zr-8Sn alloy. *Scrip. Mater.* **65**, 21–24.
- ZHAO, H. & DEBROY, T. (2001). Weld metal composition change during conduction mode laser welding of aluminum alloy 5182. *Metall. Trans.* **32B**, 163–72.